Research Article

Sanjib Majumdar*, Pankaj Kumar Singh, Ajoy Kumar Pandey, and G.V.S. Nageswara Rao

Kinetics of oxide scale growth on a $(Ti, Mo)_5Si_3$ based oxidation resistant Mo-Ti-Si alloy at 900-1300°C

https://doi.org/10.1515/htmp-2019-0056
Received Jan 07, 2019; accepted Feb 28, 2019

Abstract: High-temperature oxidation behaviour of Mo-40Ti-30Si (at.%) alloy was investigated in the temperature regime of 900-1300°C in air. Isothermal weight change data recorded up to 100 h of exposure revealed parabolic weight gain kinetics at all the tested temperatures. The protective oxide scale composed with SiO_2 (silica) and TiO_2 (titania) forming a duplex oxide microstructure consisting of TiO_2 particles embedded in the continuous SiO_2 matrix. The oxide scale showed parabolic growth kinetics, and the activation energies for the scale growth were found to be 72.2 kJ/mol in 900-1200°C and 324.9 kJ/mol in 1200-1300°C. The kinetics of the protective scale growth on the alloy surface was mainly controlled by the growth of the silica film and the inward diffusion of oxygen through the duplex oxide layer.

Keywords: High-temperature; Oxidation; Oxide scale; Kinetics; Activation energy

1 Introduction

High-temperature oxidation resistance and room temperature fracture toughness are the two key issues to be resolved for developing molybdenum based materials [1, 2] to replace nickel based superalloys used in energy producing devices operated at high temperatures. Molybdenum shows linear oxidation behaviour when exposed to air with increasing temperature [3]. The oxidation reactions follow $Mo \rightarrow MoO_2 \rightarrow MoO_3$ as the temperature is increased from room temperature. MoO_3 melts at about 795°C and it also possesses high vapour pressure at elevated temperatures. Therefore, the oxidation of Mo exhibits an initial increase in weight as the temperature is increased, and beyond certain temperature, weight loss is observed due to volatilization of MoO_3 [4]. Mo-Si-B alloy with varying composition with respect to Si and B are studied in detail [5–7]. The alloy shows improved oxidation resistance as the Si content is increased [5]. Addition of boron (B) leads to the formation of superior oxidation resistant Mo_5SiB_2 (T2) phase in the three phase Mo_{ss}-Mo_3Si-T2 microstructure. It forms a protective borosilica scale on the alloy surface. For reducing the density and improving the fracture toughness, a part of Mo was substituted with titanium (Ti) and studies were done on Mo-Ti-Si-B alloys [8–11]. Although, the alloy showed superior creep properties [8, 9], the oxidation resistance has been poor at elevated temperatures. The oxide scale mainly consisted with SiO_2-TiO_2 type porous duplex scale. Evaporation of B_2O_3 and MoO_3 through the porous SiO_2-TiO_2 leading to loss of weight was reported [9]. Severe vaporization loss of the Mo-Ti-Si-B alloy was observed with increasing temperature beyond 1100°C. Presence of B_2O_3 in silica reduces its viscosity at intermediate temperatures 800-950°C. However, beyond 950°C, B_2O_3 starts evaporating and the viscosity of the silica rich scale increases. The rate of evaporation of B_2O_3increases at higher temperatures leading to the formation of pores in the oxide scale which enhances the vaporization of MoO_3 and catastrophic oxidation. Therefore, boron-free Mo-Si-Ti alloys are investigated recently [12–14]. Ti-addition in Mo-Si system would improve the toughness and reduce the density of the materials while upgrading the oxidation performance as well. The density of the Mo-Ti-Si materials was reported to be much lower than that of conventional nickel based superalloys [14]. The stability of different phases in ternary Mo-Ti-Si system is reported earlier [15].

In the present investigation, the detailed oxidation behaviour of Mo-40Ti-30Si (in at.%) system was studied in a

***Corresponding Author: Sanjib Majumdar:** High Temperature Materials Development Section, Materials Processing and Corrosion Engineering Division, Bhabha Atomic Research Centre, Trombay, Mumbai-400085, India; Email: sanjib@barc.gov.in; sanjib731@gmail.com
Pankaj Kumar Singh: National Institute of Technology, Warangal, Telangana, 506004, India; Graduate School of Advanced Sciences of Matter, Hiroshima University, Japan, PIN-7398530
Ajoy Kumar Pandey, G.V.S. Nageswara Rao: National Institute of Technology, Warangal, Telangana, 506004, India

wide temperature regime of 900-1300°C in static air. The weight change behaviour of the alloy was recorded. The cross-section of the oxide scale was analysed using SEM and EDS. The growth kinetic of the oxide scale was evaluated. The superior oxidation resistance of the alloy was understood using microstructural observations and thermodynamic considerations.

2 Experimental

Mo-40Ti-30Si (in at.%) alloy was produced by adopting powder metallurgical processing route. Mechanical alloying of the elemental powder was carried out using a planetary ball mill. Reactive hot pressing of the alloy powder was conducted at 1600°C for producing the alloy plates. The detailed preparatory procedure for the alloy is presented earlier [14]. Figure 1 shows the back scattered electron microstructure of the hot pressed alloy. The alloy is composed of the hexagonal type matrix phase (Ti, $Mo)_5Si_3$ and (Ti, $Mo)_3Si$ precipitates (dark colour) forming a composite type microstructure. The composition and grain structures of the hot pressed alloy were reported earlier [14]. The (Ti, $Mo)_5Si_3$ phase contains Ti-34.7 at.%, Mo-26.4 at.%, Si-38.9 at.%, and (Ti, $Mo)_3Si$ precipitate is comprised with Ti-63.2 at.%, Mo-14.3 at.%, Si-22.5 at.%. The density of the alloy was measured as 5.8 g/cm^3, much lower than that of conventional nickel based superalloys.

Electro-discharge machining (EDM) equipment was used to cut the mall specimens of dimensions 10 mm × 5 mm × 5 mm from the hot pressed plates of the alloy. The specimens were subsequently ground to 1200 grit SiC embedded emery paper. All the sides of the specimens were ground and the sharp edges or corners were removed. The samples were thoroughly cleaned ultrasonically in water and acetone bath. Isothermal oxidation tests of the alloy samples were conducted at 900, 1000, 1100, 1200 and 1300°C for different time intervals ranging from 0.5 h to 100 h. The samples were kept inside the muffle type furnace using alumina boats and the weight of the boat containing the specimen was measured before and after the oxidation tests. A Sartorius make micro balance was used to measure the weight accurately. The samples were loaded inside the furnace when the required temperature was reached inside the chamber. Each sample was carefully weighed before and after exposure to determine the weight changes during the oxidation. The morphology and the composition of the oxide layer were investigated by observing the surface as well as the cross-section using a Camscan made SEM attached with Oxford EDS (Model: X-max 80). The oxidation-test samples were mounted in conducting mould applying the hot mounting procedure. The metallographic samples were prepared by grinding the mounted specimens up to 1 µm diamond finish and subsequent polishing with colloidal silica solution.

3 Results

3.1 Oxidation behaviour

Mo-40Ti-30Si alloy exhibited the gain in weight behaviour during isothermal oxidation in the temperature regime of 900-1300°C. The weight change data recorded at differ-

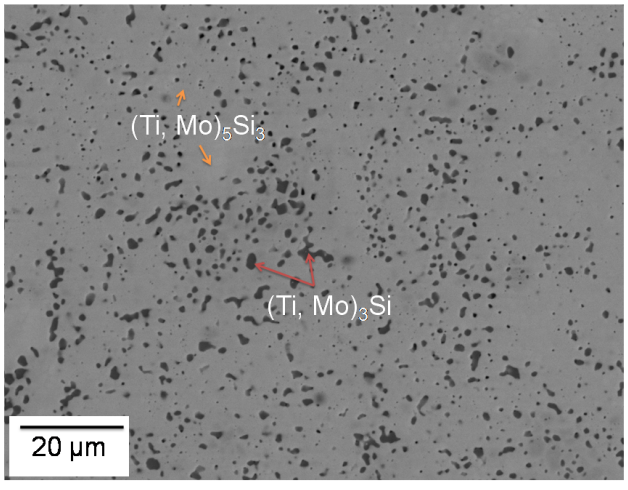

Figure 1: BSE microstructure of the Mo-40Ti-30Si system containing (Ti, $Mo)_5Si_3$ matrix and (Ti, $Mo)_3Si$ precipitates.

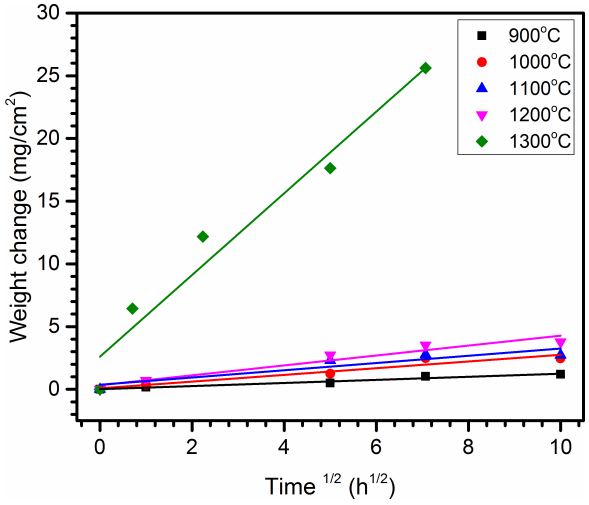

Figure 2: Weight change data indicating parabolic oxidation behaviour of Mo-40Ti-30Si in static air.

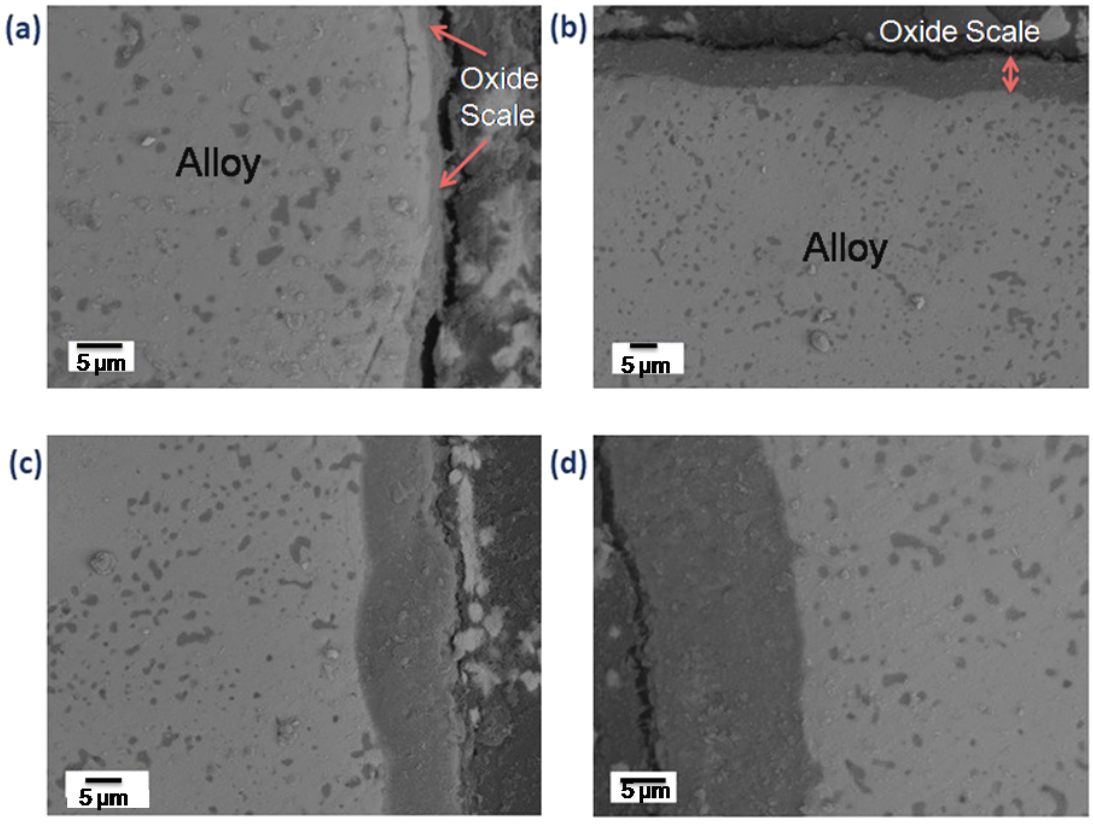

Figure 3: Cross-sectional BSE images of the Mo-Ti-Si composite oxidized at 1100°C in air for (a) 1 h, (b) 25 h, (c) 50 h and (d) 100 h.

ent time intervals under isothermal oxidation conditions are plotted as Δw vs $t^{0.5}$ in Figure 2. The weight change data for 900, 1000 and 1300°C are taken from the reference 14 for comparison. The weight change data was measured at least three times, and the error in the measured data may be considered as ±5% due to manual handling of the oxidized samples. The alloy showed superior oxidation resistance at 900-1200°C in air. Although the magnitude of weight gain increased with increasing temperature and time, the absolute value of the maximum weight gain observed at 1200°C after 100 h was found to be very low (~ 3.7 mg/cm^2). At 1300°C, a faster weight gain was observed, and the value of the weight gain after 50 h of exposure in air was of the order of 25.6 mg/cm^2. Beyond 50 h, the scale was spalling off and therefore, the weight change data could not be recorded. Therefore, the alloy showed superior oxidation resistance up to 1200°C for longer exposure times, and at 1300°C for 50 h. Curve fitting was done to understand the weight gain kinetics of oxidation of the alloy. Linear fitting of weight change (Δw) against $t^{0.5}$ in Figure 2 indicated that the weight gain kinetics followed a parabolic behaviour. The calculated weight gain rate constant values ranged between 0.12-0.39 mg/cm$^2 \cdot h^{0.5}$ in 900-1200°C with a high value of 3.25 mg/cm$^2 \cdot h^{0.5}$ at 1300°C. A drastic increase in the oxidation kinetics was observed from 1200 to 1300°C, which could be due to the mechanistic change of oxidation of the alloy in this temperature regime. The weight gain rate constant values at 1300°C were found to be about 10-15 times higher than those for 900-1200°C.

3.2 Growth of oxide scale

For accurately measuring the thickness of the oxide scales the metallographic samples were prepared using hot mounting with conducting mould. Back scattered electron image analysis is preferred as the Z-contrast between the substrate and oxide scale is clearly revealed. Figure 3 represents the BSE cross-sectional showing the oxide scale formed at 1100°C at different time intervals. The similarities are observed in the oxide scale formed at all the four temperatures between 900 and 1200°C. Therefore, the one set of micrographs from the samples tested 1100°C are presented here (in Figure 3). The thickness of the oxide scale increased with increasing the time of exposure at 1100°C. Comparing with the weight gain data presented in Figure 2, a one to one correlation could be established with the

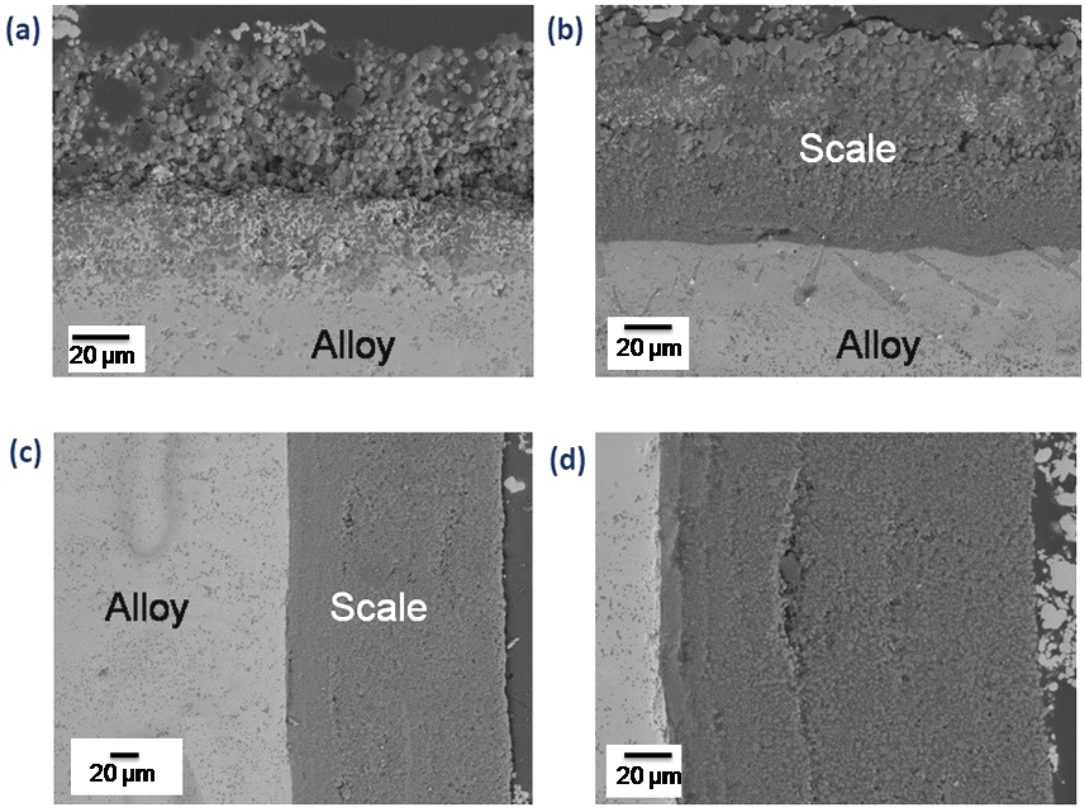

Figure 4: Cross-sectional BSE images of the Mo-Ti-Si composite oxidized at 1300°C in air for (a) 0.5 h, (b) 5 h, (c) 25 h and (d) 50 h.

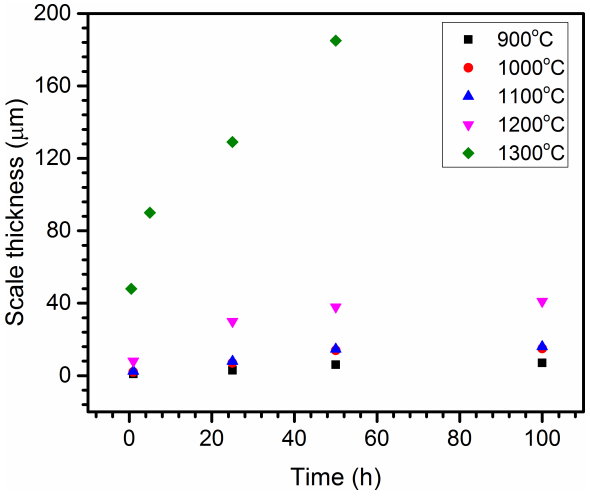

Figure 5: Variation of the thickness of the oxide scale with time at different temperatures.

gain in weight and increase in thickness of the oxide scale with time at isothermal condition. The thickness of the oxide scale varied between 1 µm and 41 µm at 900-1200°C temperature regime. The growth rate of the oxide scale was much higher at 1300°C. The cross-section of the oxide scale along with Mo-40Ti-30Si alloy substrate formed at 1300°C is presented in Figure 4. The thicknesses of the oxide scales are much higher (~185µm in 50h) at 1300°C. The values of oxide scale thickness at different times and temperatures are presented in Figure 5. The thicknesses of the oxide scales were measured at about 5 different places. The error in measurement at lower thicknesses (~1 µm) was about ±10 %, whereas for higher thicknesses the measurement was accurate the variation of thickness was in ±5 % range. The analysis of the scale thickness data revealed a parabolic scale growth kinetics obeying the following law.

$$h^2 = \mathrm{K}_1 t \tag{1}$$

or,

$$h = Kt^{1/2} \tag{2}$$

where, h is the thickness of the oxide scale, t is the time and K is the scale growth rate constant. Figure 6 shows h vs $t^{1/2}$ curves obtained from Figure 5 fitted in linear plots. The slope of the linear curves is the growth rate constant (K). Applying Arrhenius equation it follows.

$$K = K_0 \exp(-\mathrm{E}_a/\mathrm{RT}) \tag{3}$$

$$\ln K = \ln K_0 - \mathrm{E}_a/\mathrm{RT} \tag{4}$$

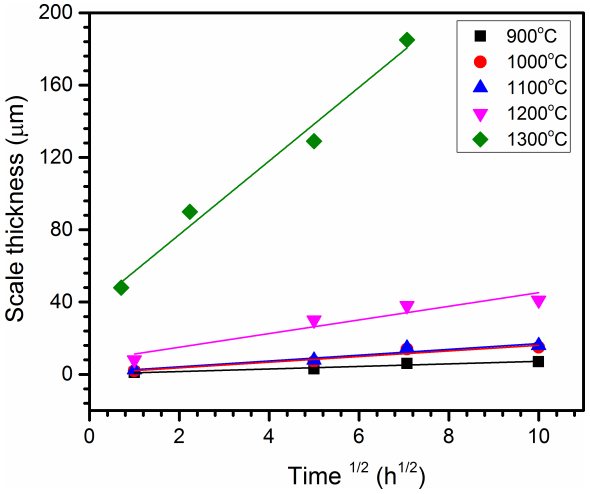

Figure 6: Scale thickness (h) vs $t^{1/2}$ plots confirming parabolic growth kinetics of the oxide scale.

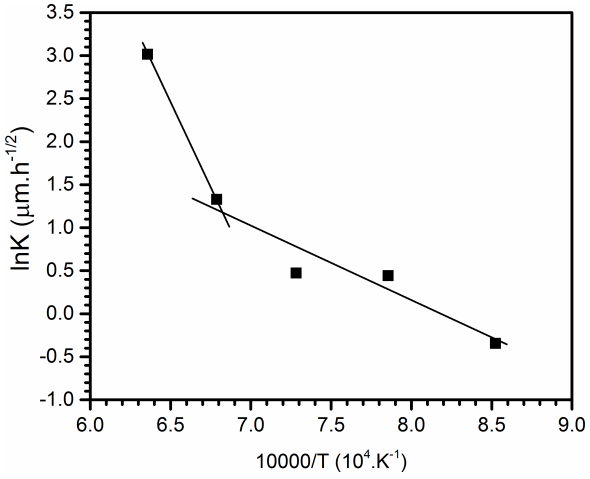

Figure 7: Arrhenius plots between scale growth rate constant and 1/T indicating two different regions of oxide scale growth.

From the slope of the *ln K* vs 1/T, the activation energy (E_a) for the oxide scale growth is determined. Arrhenius plot for scale growth is presented in Figure 7. The data points in Figure 7 show two distinct regions of linear fitting indicating the change in mechanism from 900-1200°C to 1200-1300°C. The activation energies calculated from the slopes of the plots are respectively, 72.2 kJ/mol (17.2 kcal/mol) in 900-1200°C and 324.9 kJ/mol (77.3 kcal/mol) in 1200-1300°C.

4 Discussion

The alloy Mo-40Ti-30Si is composed of a matrix phase of $(Ti, Mo)_5Si_3$ along with the second phase precipitates of

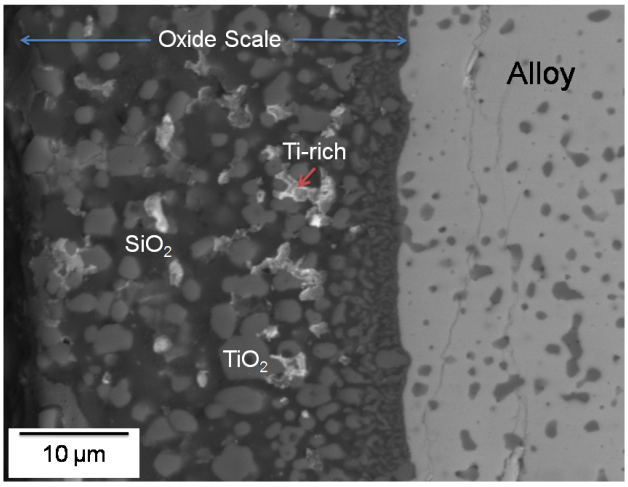

Figure 8: BSE image showing the microstructure of the oxide scale and the alloy substrate.

$(Ti, Mo)_3Si$ (Figure 1). The probable reactions occur during high-temperature exposure of the alloy in air are presented in the following.

$$(Ti, Mo)_5Si_3 + 15.5O_2 \rightarrow 5TiO_2 + 3SiO_2 + 5MoO_3 \quad (5)$$

$$(Ti, Mo)_5Si_3 + 8O_2 \rightarrow 5TiO_2 + 3SiO_2 + 5Mo \quad (6)$$

$$3(Ti, Mo)_5Si_3 + 4O_2 \rightarrow 4SiO_2 + 5(Ti, Mo)_3Si \quad (7)$$

$$(Ti, Mo)_3Si + 8.5O_2 \rightarrow 3TiO_2 + SiO_2 + 3MoO_3 \quad (8)$$

$$5(Ti, Mo)_3Si + O_2 \rightarrow 10TiO_2 + SiO_2 + (Ti, Mo)_5Si_4 \quad (9)$$

The abovementioned reactions are mainly based on stoichiometries. The reactions (5) and (8) predict the complete formation of oxides TiO_2, SiO_2 and MoO_3. MoO_3 will vaporize out at all the isothermal oxidation test conditions *i.e.* in 900-1300°C. The calculations performed using stoichiometric composition predict a net weight loss of the order of 11.14 mg per oxidation of 100 mg of Mo-40Ti-30Si (at.%) alloy. However, all the isothermal oxidation data (Figure 2) showed weight gain behaviour. Therefore, oxidation of molybdenum forming MoO_3 is suppressed. The probability of the occurrence of the reactions (6), (7) and (9) is higher during the oxidation of the alloy.

Figure 8 represents a clearer image of the oxide scale. The scale mainly consists of dark colour SiO_2 (silica) matrix in which brighter TiO_2 (titania) particles are embedded. The presence of these phases was confirmed by quantitative EDS analysis and XRD [14]. The brightest particles (marked as Ti-rich) in Figure 8 were found to be composed

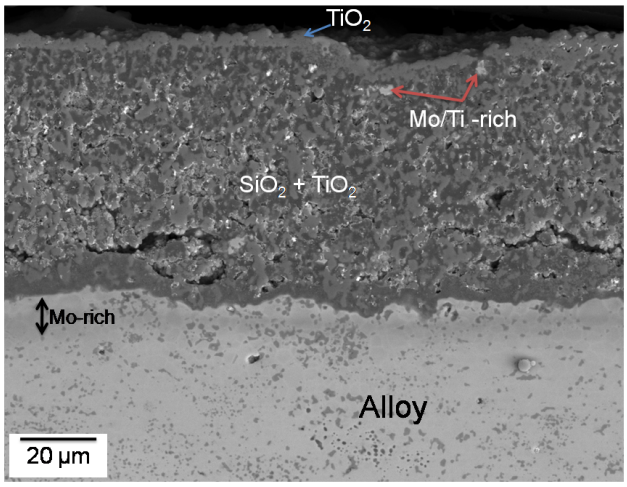

Figure 9: Cross-sectional BSE image indicating the presence of a TiO_2 rich thin outer layer, and a Mo-rich layer at the scale/alloy interface.

of two type of compositions namely Ti-50.9, Mo-22.1, Si-27.0 (in at.%) ((Ti, Mo)$_3$Si type) and Ti-49.6, Si-50.4 ((Ti, Mo)$_5$Si$_4$ type). The standard deviation of EDS composition analysis data presented here may be considered as 1 at.% for each element. These analytical results also confirm the oxidation mechanisms following the reactions (7) and (9). Figure 9 shows a BSE image of the scale/substrate cross-section obtained at 1200°C. A thin TiO_2 rich layer is present at the outer layer. The oxide scale is mainly composed with duplex SiO_2 (TiO_2) oxides. The presence of very fine size bright particles rich in Ti or Mo is also detected throughout the oxide scale. Figure 10 represents a cross-sectional image and EDS X-ray maps for the elements Mo La, Ti Ka, Si Ka and O Ka. EDS maps clearly reveal that O Ka (Figure 10d) is present in the whole area of the scale. Si Ka and Ti Ka spots are clearly demarcated separately in Figures 10(b) and (c), respectively. Figure 10(e) indicates the presence of Mo-rich particles in the oxide scale and enrichment of Mo at the scale/alloy interface. The quantitative EDS analysis at the scale/alloy interface indicates the presence of Si-41.6, Ti-29.8, Mo-28.6 (in at.%) forming a Mo-rich (Ti, Mo)$_5$Si$_4$ type phase at the interface. Therefore, some amount of Mo is released through the reaction (6), which gets distributed in the silicide phases.

Thermodynamic stability of different oxides such as TiO_2, SiO_2, MoO_3, and MoO_2 are compared. The values of standard free energy of formation at 900°C are −171.13 kcal/mol, −162.89 kcal/mol, −105.01 kcal/mol, and −85.56 kcal/mol, respectively, for TiO_2, SiO_2, MoO_3, and MoO_2. At 1300°C, the respective free energy values are −158.06 kcal/mol, −150.59 kcal/mol, −91.87 kcal/mol, and −73.59 kcal/mol. The negative free energy values indicate all the oxides are stable at these temperatures. The tendency of formation of the oxides will follow the pattern TiO_2 > SiO_2 > MoO_3 > MoO_2. The values of free energy of formation for TiO_2 and SiO_2 are much lower than those for MoO_3 and MoO_2. Therefore, the formation of a duplex oxide comprising of TiO_2-SiO_2 is more probable. The absence of MoO_3 or MoO_2 in the oxide scale is attributed to two reasons; (1) mobility of Mo in hexagonal (Ti, Mo)$_5$Si$_3$ phase is low and (2) the activity or chemical potential (driving force) for Mo oxide formation is lower. It is reported [13] that the migration barrier of Ti is much lower compared to that of Mo in (Mo, Ti)$_5$Si$_3$ silicides. Ti diffuses through Mo vacancies and Ti is more mobile than Mo. The mobility of Si is also more in these systems. The driving forces for Ti to form TiO_2 and Si to form SiO_2 are comparable. Oxidation behaviour of titanium silicide based systems was studied in detail [16–20]. It was reported that the Si concentration of 39 at.% stabilizes SiO_2 over TiO_2 in the Ti-Si-O system when the oxygen partial pressure is very low [20]. However, both TiO_2 and SiO_2 are formed in air atmosphere.

The growth of the duplex SiO_2 (TiO_2) layer on the Mo-40Ti-30Si alloy is pretty interesting. From the microstructures (Figures 3, 4, 8, 9, 10) of the oxide scale, it is clearly understood that SiO_2 is forming a sort of matrix type phase in which TiO_2 particles are embedded. The whole structure grows with simultaneous formation of both the oxides keeping the scale intact with the substrate alloy. No porosities or cracks are noticed in the scale up to 1200°C. Pure titanium oxidises intensively beyond 500°C in air by absorbing oxygen and nitrogen [21]. TiO_2 crystals are formed on the surface of Ti, and the oxide layer is non-protective beyond 700°C forming a porous powdery structure. Non-stoichiometric TiO_2 is a metal excess n-type semiconductor, and it shows good conductivities (electronic and ionic) even at lower partial pressure of oxygen [22]. On the contrary, thermal oxidation of Si produces a thin to thick SiO_2 layer which is protective in nature up to very high temperatures. Beyond 1250°C, SiO_2 becomes amorphous and less viscous. Kinetics of oxidation of Si is reported to linear to parabolic and growth of oxide layer following parabolic kinetics [23, 24]. The activation energy for silica scale growth in 900-1200°C was reported to be 28.5 kcal/mol [23]. The activation energy obtained in the current investigation is slightly lower (17.2 kcal/mol) than that of pure silica. This is attributed to the presence of TiO_2 particles in the silica phase. However, the reported activation energy for wet-oxygen oxidation of Si is 16.3 kcal/mol [23]. The mechanisms for the scale growth follow three stages; (1) transport of oxygen from air to the outer surface where it is adsorbed, (2) oxygen atoms or ions are transported across the oxide film towards the alloy, (3) reaction at the alloy sur-

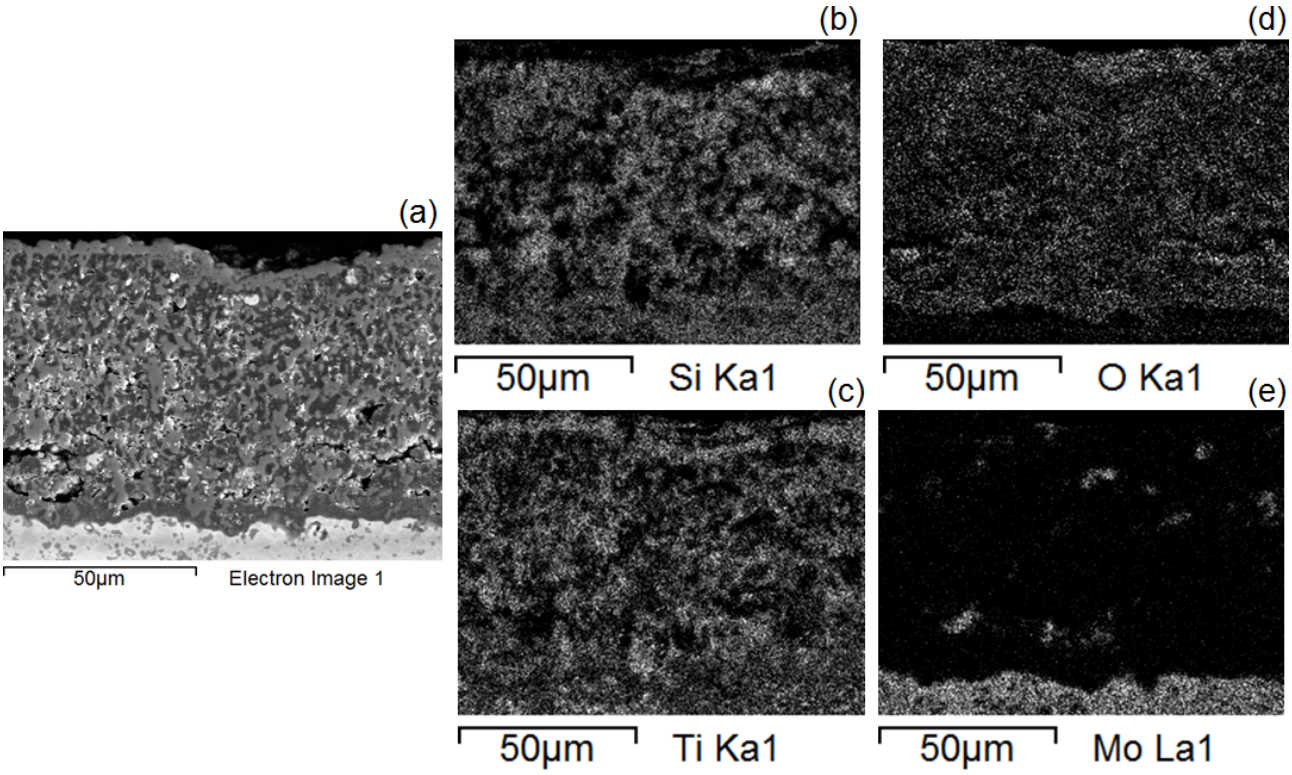

Figure 10: (a) Cross-sectional BSE image and EDS X-ray maps across the scale/alloy interface for (b) Si Ka, (c) Ti Ka, (d) O Ka and (e) Mo La.

face forming a new layer of SiO_2 (TiO_2). The activation energies for diffusion of oxygen and water through fused silica are reported to be 27.0 kcal/mol and 18.3 kcal/mol, respectively [23]. These values are in reasonably good agreement with activation energy of the scale growth. Therefore, the growth of the duplex protective oxide scale on Mo-40Ti-30Si is mainly controlled by the growth of the matrix silica phase by inward diffusion of oxygen.

The accelerated scale growth was observed in 1200-1300°C with a much higher value of activation energy (77.3 kcal/mol). This could be due to the change of the structure in the silica accelerating the inward diffusion rate of oxygen. The fraction of TiO_2 phase increases in the duplex scale formed at 1300°C (Figure 4) with increasing time of exposure. This leads to the creation of stresses at the interfaces between SiO_2 and TiO_2 forming porosities and cracks in the oxide layer. However, the oxide layer remained protective up to 50 h of oxidation at 1300°C in air. (Mo, Ti)Si_2 coatings are reported to improve the oxidation resistance further up to 1500°C [25]. Therefore, the development of multi-phase Mo-Ti-Si-X alloys possessing superior creep properties [26] and good oxidation resistance would be the focus of further studies.

5 Conclusions

Mo-40Ti-30Si (at.%) alloy comprised of (Ti, $Mo)_5Si_3$ matrix with (Ti, $Mo)_3Si$ precipitates having a low density (5.8 g/cm^3) is a promising material for high-temperature application beyond nickel based superalloys. The alloy showed superior oxidation resistance at 900-1300°C in air. The detailed isothermal oxidation tests conducted at 900, 1000, 1100, 1200 and 1300°C revealed parabolic weight gain behaviour with the time of exposure up to maximum of 100 h. The oxide scale structure analysed in detail using SEM and EDS exhibited duplex oxide layer comprising with SiO_2 matrix with dispersion of TiO_2 particles. Formation and volatilization of MoO_3 was hindered due to the formation of the continuous silica layer as matrix and titania as precipitate type morphology in the oxide scale. The growth of the oxide layer followed parabolic kinetics. Arrhenius plots for scale growth rate constant versus temperature showed two regions between 900-1200°C and 1200-1300°C indicating the change in mechanisms at higher temperatures due SiO_2 becoming amorphous. The calculated activation energy values for scale growth matched well with the reported values for growth of the silica layer. Hence, the dominance of silica formation maintained the oxide

layer continuous, adherent and protective at high temperatures.

References

[1] D. M. Dimiduk and J. H. Perepezko, MRS Bulletin, 28 (2003) 639-645.
[2] J. A. Lemberg and R. O. Ritchie, Advanced Mater., 24 (2012) 3445-3480.
[3] G. R. Smolik, D. A. Petti, and S. T. Schuetz, J. Nucl. Mater., 283-287 (2000) 1458.
[4] S. Majumdar and I. G. Sharma, Intermetallics, 19 (2011) 541-545.
[5] M. K. Meyer and M. Akinc, J. Amer Ceram. Soc., 79 (1996) 938-944.
[6] M. G. Mendiratta, T. A. Parthasarathy, and D. M. Dimiduk, Intermetallics, 10 (2002) 225-232.
[7] S. Majumdar, B. Gorr, H.-J. Christ, D. Schliephake, and M. Heilmaier, Corrosion Sci., 88 (2014) 360–371.
[8] D. Schliephake, M. Azim, K. v. Klinski-Wetzel, B. Gorr, H.-J. Christ, H. Bei, et al., Metall. Mater. Trans. A, 45 (2014) 1102-1111.
[9] M. Azim, D. Schliephake, C. Hochmuth, B. Gorr, H.-J. Christ, U. Glatzel, et al., JOM, 67 (2015) 2621-2628.
[10] T. Moriyama, K. Yoshimi, M. Zhao, T. Masnou, T. Yokoyama, J. Nakamura, et al., Intermetallics, 84 (2017) 92–102.
[11] M. Zhao, S. Nakayama, T. Hatakeyama, J. Nakamura, and K. Yoshimi, Intermetallics, 90 (2017) 169–179.
[12] S. Burk, B. Gorr, H.-J. Christ, D. Schliephake, M. Heilmaier, C. Hochmuth, et al., Scripta Mater., 66 (2012) 223–226.
[13] M. A. Azim, B. Gorr, H.-J. Christ, O. Lenchuk, K. Albe, D. Schliephake, et al., Intermetallics, 90 (2017) 103–112.
[14] S. Majumdar, B. Paul, P. Kumar Singh, J. Kishor, and V. Kain, Intermetallics, 100 (2018) 126–135.
[15] Y. Yang, Y. A. Chang, L. Tan, and Y. Du, Mater. Sci. Eng. A, 361 (2003) 281-293.
[16] Z. Tang, J. J. Williams, A. J. Thom, and M. Akinc, Intermetallics, 16 (2008) 1118-1124.
[17] R. Mitra and V. V. Rama Rao, Metall. Mater. Trans. A, 29 (1998) 1665-1675.
[18] A. Abba, A. Galerie, and M. Caillet, Oxid. Metals, 17 (1982) 43-54.
[19] D. Vojtěch, B. Bártová, and T. Kubatík, Mater. Sci. Eng. A, 361 (2003) 50-57.
[20] J. I. Goldstein, S. K. Choi, F. Van Loo, G. F. Bastin, and R. Metselaar, J. Am. Ceram. Soc., 78(2) (1995) 313–322.
[21] K. Aniołek, Vacuum, 144 (2017) 94-100.
[22] R. N. Blumenthal, J. Baukus, and W. M. Hirthe, J. Electrochem. Soc., 114 (1967) 172-176.
[23] B. E. Deal and A. S. Grove, J. Appl. Phys., 36 (1965) 3770-3778.
[24] A. G. Revesz, B. J. Mrstik, H. L. Hughes, and D. McCarthy, J. Electrochem. Soc., 133 (1986) 586-592.
[25] W. Li, J. Fan, Y. Fan, L. Xiao, and H. Cheng, J. Alloys Comp., 740 (2018) 711-718.
[26] D. Schliephake, A. Kauffmann, X. Cong, C. Gombola, M. Azim, B. Gorr, et al., Intermetallics, 104 (2019) 133–142.